Can the Intermediate Western Boundary Current recirculation trigger the Vitória Eddy formation?

As Published: https://doi.org/10.1007/s10236-020-01437-6

Publisher: Springer Berlin Heidelberg

Persistent URL: https://hdl.handle.net/1721.1/131994

Version: Author's final manuscript: final author's manuscript post peer review, without publisher's formatting or copy editing

Can the Intermediate Western Boundary Current recirculation trigger the Vitória Eddy formation?

Cite this article as: Dante C. Napolitano, Cesar B. Rocha, Ilson C. A. da Silveira, Iury T. Simoes-Sousa and Glenn R. Flierl, Can the Intermediate Western Boundary Current recirculation trigger the Vitória Eddy formation?, *Ocean Dynamics* doi: 10.1007/s10236-020-01437-6

Ocean Dynamics manuscript No.
(will be inserted by the editor)

Can the Intermediate Western Boundary Current recirculation trigger the Vitória Eddy formation?

Dante C. Napolitano · Cesar B. Rocha · Ilson C. A. da Silveira · Iury T. Simoes-Sousa · Glenn R. Flierl ·

Received: date / Accepted: date

Abstract South of the Vitória-Trindade Ridge, a seamount chain off East Brazil, the Brazil Current (BC) meanders cyclonically within Tubarão Bight, occasionally forming the Vitória Eddy. It was recently found that the Intermediate Western Boundary Current (IWBC), which flows equatorward below the BC, cyclonically recirculate within Tubarão Bight. We present an analysis of AVISO observations that suggest that the Vitória Eddy formation is conditioned by the strength of the BC upstream of Tubarão Bight. A weak BC is prone to local meandering and eddy formation in the bight, while a strong BC suppresses eddy formation in the bight but triggers downstream meander growth. To study the effects of the IWBC recirculation on the BC meandering and the Vitória Eddy formation, we formulate a simple two-layer quasi-geostrophic model. In the model, the BC is represented by a meridional jet in the upper layer and the IWBC recirculation is a steady eddy in the lower layer. The lower-layer eddy effectively acts as a topographic bump, affecting the upper-layer jet via the stretching term ψ_2/R_d^2, where ψ_2 is the lower-layer streamfunction and R_d is the baroclinic deformation radius. Based on the AVISO sea-surface height data and previous observational studies, we define a stationary eddy and reference jet. We conduct a number of initial-value problem experiments varying the upper-layer jet speed. A weak upper-layer jet slowly meanders and develops a cyclone above the lower-layer eddy. As we increase the jet velocity, the meandering is faster and the cyclone is larger. But a too-strong jet has an opposite effect: the potential vorticity anomalies induced by the lower-layer

Dante C. Napolitano (ORCID 0000-0001-9857-9724)
Instituto Oceanográfico, Universidade de São Paulo, São Paulo, SP, Brazil
E-mail: dante.napolitano@alumni.usp.br

Cesar B. Rocha (ORCID 0000-0003-4063-5468)
University of Connecticut, Avery Point, Groton, CT

Ilson C. A. Silveira (ORCID 0000-0001-9266-6480)
Instituto Oceanográfico, Universidade de São Paulo, São Paulo, SP, Brazil

Iury T. Simoes-Sousa (ORCID 0000-0002-2484-510X)
University of Masssachusetts Dartmouth, North Dartmouth, Massachusetts, USA

Glenn R. Flierl (ORCID 0000-0003-3589-5249)
Massachusetts Institute of Technology, Cambridge, Massachusetts, USA

eddy are quickly swept away, leading to explosive downstream meander growth; no cyclone is formed above the lower-layer eddy. In all cases, the initial meandering trigger is a linear process (the steering of the upper-layer jet by the lower-layer eddy). But even when the upper-layer jet is weak, nonlinearity quickly becomes important, dominating the dynamics after 10 days of simulation. The downstream meander growth is fully nonlinear. Our idealized QG model confirms that the IWBC recirculation can trigger the Vitória Eddy formation and elucidates the mechanisms involved in this process.

Keywords Brazil Current · Vitória Eddy · two-layer model · flow over topography · Dedalus

1 Introduction

The Brazil Current (BC) is the subtropical western boundary current of the South Atlantic. The BC is formed at about 15 °S, developing quasi-stationary, recurrent anticyclones as it negotiates the Brazilian eastern continental margin (Soutelino et al., 2011). At 20 °S, the BC encounters the Vitória-Trindade Ridge, a zonal seamount chain.

The Abrolhos Bank and seamounts act as physical obstacles to the BC as it crosses the Vitória-Trindade Ridge poleward (see figure 1). South of the Vitória-Trindade Ridge, the BC meanders within Tubarão Bight, sometimes forming the Vitória Eddy (cf. Schmid et al., 1995). In the first description of the Vitória Eddy, Schmid et al. (1995) attributed its formation to the BC meandering, which was linked to strong coastal upwelling events. This topographically constrained eddy is quasi-stationary, with rare equatorward-translation events, first described by Campos (2006) using a numerical simulation. Arruda et al. (2013) attributed those Vitória Eddy translation events to dipole interactions with the Abrolhos Eddy (cf. Soutelino et al., 2011).

Flowing equatorward at intermediate layers, the Intermediate Western Boundary Current (IWBC; cf. Boebel et al., 1999), originating at 28 °S, reaches Tubarão Bight, forming a topographically forced cyclonic recirculation (Costa et al., 2017). This recirculation—hereafter the IWBC Eddy—is quasi-steady and constrained to Tubarão Bight. In other words, the recirculation barely changes its speed or its position in time compared to the time scale of the BC variability (see Costa et al., 2017; Napolitano et al., 2019, for details).

Interactions between the BC and the IWBC have been studied by Silveira et al. (2008), Mano et al. (2009) and Rocha et al. (2014). Silveira et al. (2008) showed that the meandering of the BC-IWBC system is caused by baroclinic instability. Using a numerical model, Mano et al. (2009) estimated baroclinic conversion during a cyclonic meandering event, showing that the perturbation starts at the IWBC and transfers energy from intermediate to upper layers as it grows. Based on the analysis of three moorings along the BC axis, Rocha et al. (2014) showed that the mean-to-eddy baroclinic conversion peaks around the BC-IWBC interface. The effects of a topographically-forced, slower-varying deep flow driving changes in the upper layers have also been addressed by Hurlburt and Hogan (2008), for the Gulf Stream separation region, and by Hurlburt et al. (2008), for the Japan/East Sea.

Given the formation site of the intermittent, quasi-standing Vitória Eddy located above the quasi-permanent, stationary IWBC Eddy, we ask: Is the stretching produced by the IWBC recirculation strong enough to deflect the BC in the upper layers? In other words, how the IWBC Eddy affects the formation of the Vitória Eddy?

As an initial step toward answering this question, we first look at the BC in the upper layer. We examine 26 years of altimetry data to identify (i) the path and velocity of the BC within Tubarão Bight; and (ii) the conditions sustaining or hindering the Vitória Eddy formation.

2 Altimeter observations within Tubarão Bight

Sea surface height (SSH) contours can be used as a proxy for the geostrophic signature of the western boundary currents (Vallis, 2017). To determine the main axis of the Kuroshio, Qiu and Chen (2005) used the 170-cm contour based on the maximum SSH meridional gradient in the region, whereas Andres (2016), using the same approach, selected the 25-cm contour for the Gulf Stream.

Here, we use the SSH contours from the AVISO dataset, distributed by the Copernicus Marine Environment Monitoring Service (CMEMS), at L4-level processing with $1/4^\circ$ of horizontal resolution. (The data are available at www.aviso.altimetry.fr/duacs.)

BC axis position and velocity

In our study region, we choose the 59-cm contour as a proxy for the BC axis streamline. This contour represents the approximate location of the maximum SSH gradient throughout the region. Figure 1 shows the BC paths, as indicated by the 59-cm SSH contours, obtained from 26 years of AVISO data. The blue lines depict the paths obtained from monthly-averaged SSH fields, and the red line is based on the 26-year average SSH. (South of 21 °S, we only considered contours in regions shallower than the 3500-m isobath.) In the upper layer, nearly every BC streamline crosses Tubarão Bight through the center of the intermediate-layer IWBC Eddy—the dashed black line in figure 1, which is based on Costa et al. (2017) and Napolitano et al. (2019). While monthly means in figure 1 show significant spreading of the BC paths north of 22 °S, there is much less variability south of 22 °S, where the BC organizes itself.

From daily altimeter-derived geostrophic velocity we calculated the maximum velocity within Tubarão Bight. Figure 2-A displays a timeseries of the mean along-axis BC velocity above the IWBC Eddy. The mean BC speed within Tubarão Bight is $0.2\,\mathrm{m\,s^{-1}}$, ranging from $\sim$0.1 to $0.5\,\mathrm{m\,s^{-1}}$. Panel B shows the probability density function (PDF) of the BC speed, with frequent weak values close to half the mean, and episodic high velocities more than twice the mean. Previous mooring data in the region depicted mean velocities in the same ballpark as our estimates for the BC: in the Vitória-Trindade Ridge's main channel, Müller et al. (1998) reported $0.09\,\mathrm{m\,s^{-1}}$; within Tubarão Bight, Costa et al. (2017) reported $0.09\pm0.02\,\mathrm{m\,s^{-1}}$; downstream the bight, Rocha et al. (2014) reported $0.31\pm0.12\,\mathrm{m\,s^{-1}}$ at 22.8 °S. The maximum daily-velocity estimates in figure 2 is about $0.5\,\mathrm{m\,s^{-1}}$, close to shipboard-ADCP velocities in the Vitória-Trindade Ridge reported by Napolitano et al. (2019). Schmid et al. (1995) also found similar values within the innermost

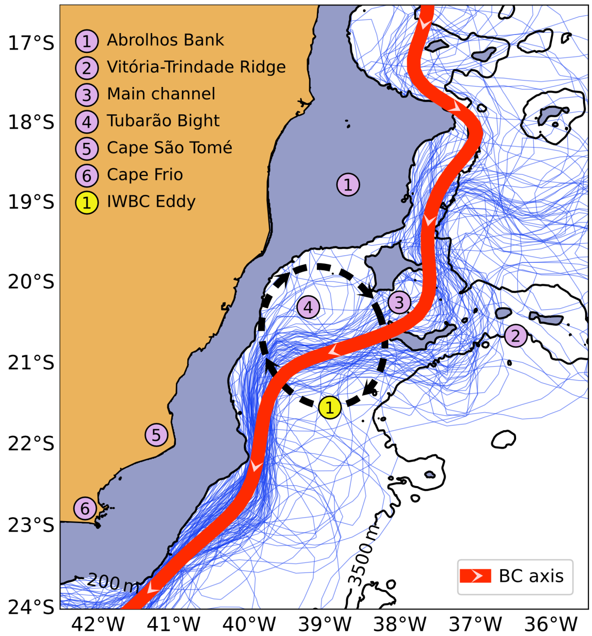

Fig. 1 Southeastern Brazil main topographic features and the Brazil Current axis. The current axis is represented by the 59-cm SSH contours (from 1993 to 2018) over a schematic IWBC eddy. Blue lines represent the 59-cm contour on monthly SSH means; the red line represents the 59-cm contour in the mean SSH for the whole series. The IWBC eddy is represented by the black dashed ellipse.

part of Tubarão Bight, using hydrographic sections and surface drifters. Off Cape Frio (23 °S), Silveira et al. (2004, 2008) analyzed data from synoptic velocity profilers and a mooring, and found maximum velocities of $0.5\,\mathrm{m\,s^{-1}}$ and $0.41\,\mathrm{m\,s^{-1}}$, respectively.

Vitória Eddy formation and suppression events

We define three BC regimes according to figure 2: the WEAK BC, with a velocity of $0.1\,\mathrm{m\,s^{-1}}$; the MEAN BC, with $0.2\,\mathrm{m\,s^{-1}}$; and the STRONG BC, with $0.5\,\mathrm{m\,s^{-1}}$. Following this classification, we examined the AVISO timeseries and selected, for each regime, periods of 30 days in which the BC crossed Tubarão Bight above the center of the IWBC Eddy, assuming that the eddy is stationary and thus remains locked within the bight. (Since we use gridded geostrophic velocities, this classification may underestimate the BC strength during the events described next.) Analyzing AVISO's daily SSH, we find that both local and remote mesoscale eddies are responsible for the variability in Tubarão Bight (e.g., Mill et al., 2015). To isolate the local effects, we selected periods where remotely-generated perturbations rarely entered the region, i.e. periods that the Vitória Eddy formation resulted solely from the BC meandering. Figure 3 shows snapshots of these events for each of the BC regimes defined above.

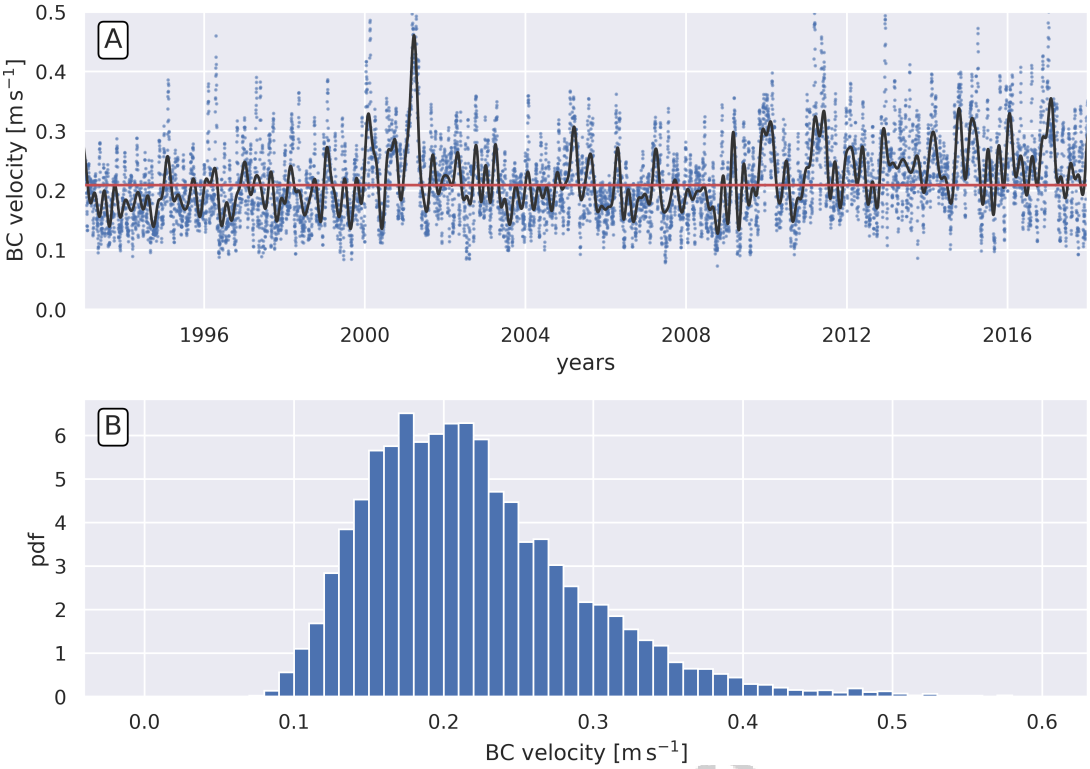

Fig. 2 (A) Timeseries and (B) pdf for the Brazil Current geostrophic velocity within Tubarão Bight from AVISO altimetry. Blue dots represent daily velocity values; the black line represents the low-pass filtered velocity (60 days); the red solid line represents the mean velocity during the whole series.

On 21 May 1999, a WEAK BC enters Tubarão Bight through the Vitória-Trindade Ridge's main channel, flowing poleward along the Abrolhos Bank, and partially meandering in a cyclonic loop centered at ∼21.5 °S–37 °W (figure 3-A). Although fully developed on 31 May, an asymmetric Vitória Eddy with a stronger oceanic lobe is shown in figure 3-B; north of the Vitória-Trindade Ridge, the BC is not well organized. Figure 3-C shows the stationary Vitória Eddy within the IWBC Eddy domain, and mesoscale activity in the shelf break around Cape Frio (e.g., Silveira et al., 2008). North of the Vitória-Trindade Ridge, the BC reorganizes starting on 16 June (see figure 3-C).

On 22 February 2015 a MEAN BC crosses the Vitória-Trindade Ridge mainly through its innermost channel (see figure 3-D). The BC meanders cyclonically, resulting in the Vitória Eddy. An anticyclone organizes itself north of the Vitória-Trindade Ridge at ∼19.5 °S, and a meander grows downstream of Cape São Tomé. By 9 March the Vitória Eddy is well developed (figure 3-E), and it remains coherent at least until 24 March (figure 3-F); on 24 March a cyclone is also formed from the downstream meandering (the eddies's names are referenced in figure 3).

Flowing poleward through the main channel of the Vitória-Trindade Ridge, on 24 February 2011 a STRONG BC crosses straight through Tubarão Bight, reattach-

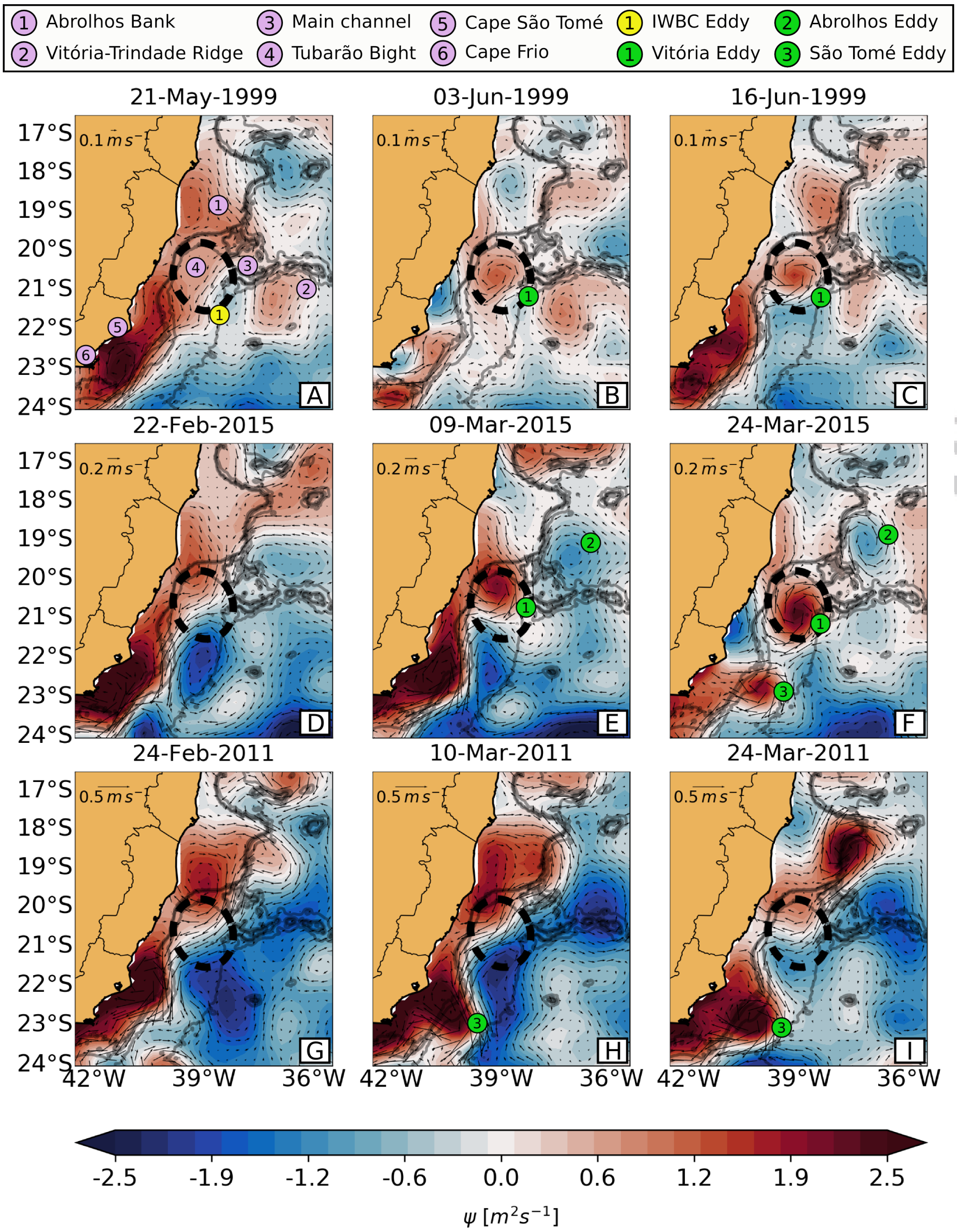

Fig. 3 Snapshots for ∼30 days of AVISO SSH corresponding to (A–C) a WEAK BC with $\sim 0.1\,\mathrm{m\,s^{-1}}$ on 21 May 1999; (D–F) a MEAN BC with $\sim 0.2\,\mathrm{m\,s^{-1}}$ on 22 Feb 2015; and (G–I) a STRONG BC with $\sim 0.5\,\mathrm{m\,s^{-1}}$ on 24 Feb 2011. Velocities are computed within Tubarão Bight. Purple keys represent the topographic features, the dashed ellipse (yellow key) marks the position of the permanent IWBC Eddy, and green keys mark the mesoscale eddies.

ing to the slope at 21 °S (see figure 3-G). This strong jet continues along the shelf break through Cape São Tomé, where a cyclonic meander grows (figure 3-H). In Tubarão Bight, the BC appears to suppress the formation of the Vitória Eddy. Downstream, at the capes, figure 3-I shows a fully-developed cyclone.

In addition to the cyclones highlighted above, anticyclonic features in figures 3-E and F (the Abrolhos Eddy) appear associated with the BC. Before the formation of the Abrolhos Eddy in figure 3-D, a large anticyclone appears east of the BC, between ∼21–23 °S. As the Vitória Eddy grows, it displaces this anticyclone poleward, until it is no longer seen in figure 3-F. In figures 3-G and H, we observe the same structure, but without the formation of the Vitória Eddy. The anticyclone endures until the end of the analyzed period, although it weakens with time.

In the different AVISO sequences analyzed, the Vitória Eddy lasts for less than 2 months. The eddy is either absorbed by the BC, or decays close to the topography of Tubarão Bight and the Vitória-Trindade Ridge. As mentioned earlier, rare equatorward-translation events of the Vitória Eddy have also been described in the literature (e.g. Campos, 2006; Arruda et al., 2013).

Motivated by these AVISO observations, from which we obtained different BC conditions in which the Vitória Eddy is formed or suppressed, we hypothesize (i) that the IWBC Eddy influences the formation of the Vitória Eddy and (ii) that the BC strength affects this process. To test these hypotheses, in section 3 we formulate a quasi-geostrophic model to simulate the interaction of the IWBC Eddy with the BC in different regimes. This simple model isolates the effects of the stretching vorticity, which couples the IWBC Eddy with the BC jet. We study the eddy generation in the upper layer by fixing the lower-layer eddy amplitude and varying the upper-layer jet strength.

3 The quasi-geostrophic model

Model equations

In our model, the evolution of the upper-layer potential vorticity (PV) in the $f-$plane is given by

$$q_t + J\left(\psi, q\right) = \nu \nabla^4 \psi \,, \tag{1}$$

where the PV is

$$q = \underbrace{\nabla^2 \psi}_{\stackrel{\text{def}}{=}\zeta} + \frac{\psi_2 - \psi}{R_d^2} \,. \tag{2}$$

Above, ψ is the upper-layer streamfunction, ψ_2 is a steady streamfunction that represents the lower-layer flow, and R_d is the baroclinic deformation radius. The Jacobian in (1) is $J(\psi, q) = \psi_x q_y - \psi_y q_x$, and the Laplacian operator in (2) is $\nabla^2 = \partial_x^2 + \partial_y^2$. To ensure numerical stability, we included the dissipative term on the right of (1), where $\nabla^4 = \nabla^2\nabla^2$ and ν is an effective viscosity.

In this simple model, the steady lower-layer flow is coupled with the upper-layer dynamics via the stretching term—the second term on the right of (2). To simulate the effects of the topographically constrained IWBC recirculation on the BC eddy formation above, we choose ψ_2 as a radially symmetric eddy (details below). We emphasize that $\psi_2 = \psi_2(x, y)$ and the dynamics in the lower layer is completely ignored. Thus (1)-(2) is effectively a barotropic quasi-geostrophic model with a topographic anomaly given by $h_b/H = \psi_2/f_0R_d^2$, where f_0 is the Coriolis parameter and H is the layer depth.

Assuming a steady state for the upper layer with $q_t = 0$, a linearized and inviscid form of (1) yields parallel streamfunction in the upper and lower layers,

$$J(\psi, \psi_2) = 0\,, \tag{3}$$

which implies $\nabla\psi \times \nabla\psi_2 = 0$, i.e. that the upper layer flow adjusts to the steady lower layer flow, or the bottom topography.

We solve (1)-(2) numerically using Dedalus (Burns et al., 2019), a framework for solving partial differential equations with standard spectral methods. We use a re-entrant channel configuration, with a Fourier basis for the along-channel y-axis, and a Chebyshev basis for the cross-channel x-axis. We prescribe the initial streamfunction ψ, calculate q in (2) at $t = 0$, and then iterate the time-marching of q with (1) and the inversion for ψ with (2). Time-stepping is performed with a fourth-order implicit-explicit Runge–Kutta scheme. We enforce no-normal flow at the channel walls:

$$\psi_y = 0 \quad \text{for} \quad n \neq 0\,, \tag{4}$$

where n is the Fourier component. As with all quasi-geostrophic channel models, the zeroth-Fourier component requires Phillips's boundary conditions (Phillips, 1954; McWilliams, 1977) given by

$$\psi_{yt} - \nu\nabla^2\psi_y = 0 \quad \text{for} \quad n = 0\,. \tag{5}$$

At the channel walls, we also enforce

$$\nabla^4\psi = 0\,, \tag{6}$$

implying that there is no vorticity diffusion through the boundaries.

Model setup and initial conditions

We run a set of initial-value experiments initialized with a jet in the upper layer that represents the Brazil Current basic state. The steady lower-layer flow is a radially symmetric eddy whose velocity is given by

$$V(r) = v_e \tanh\left(\frac{\pi r}{5\, r_e}\right) B(r)\,, \tag{7}$$

where $r = \sqrt{(x - x_c)^2 + (y - y_c)^2}$ is the radial distance from the center of the eddy (x_c, y_c), and v_e and r_e are the IWBC Eddy maximum velocity and radius, respectively, obtained from previous studies (see below). Also in (7), $B(r)$ is a bell function,

$$B(r) = \left[\frac{2}{5} + \left(\frac{r}{r_e}\right)^{15}\right]^{-1}\,. \tag{8}$$

The asymmetric eddy shape in (7) is inspired by observations that depicted an IWBC Eddy with a faster decay toward the continental slope (Costa et al., 2017;

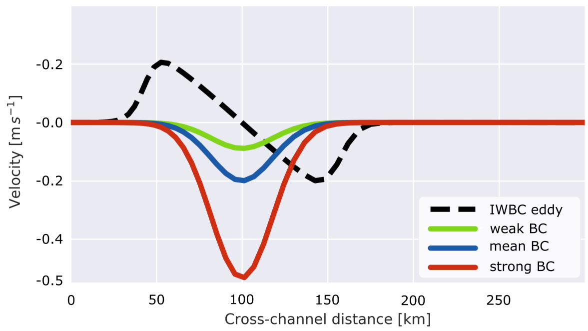

Fig. 4 Velocity profiles of the model across the center of the eddy. The dashed line shows the simulated IWBC Eddy velocity in the lower layer. Solid lines represent the simulated BC in the upper layer: (i) the green line represents the WEAK BC case; (ii) the blue line represents the MEAN BC case; and (iii) the red line represents the STRONG BC case.

Napolitano et al., 2019). Based on Napolitano et al.'s Argo climatological fields, we choose $r_e = 90\,\mathrm{km}$ and $v_e = 0.2\,\mathrm{m\,s^{-1}}$. These parameters are also consistent with values reported by Costa et al. (2017).

From $V(r)$ we compute the Cartesian x-y velocity components

$$(u, v) = V\,(\cos\theta\,, \sin\theta)\,, \tag{9}$$

where $\theta = \tan^{-1}[(y - y_c)/(x - x_c)]$. The streamfunction ψ_2 is calculated numerically given u and v, using an iterative method in Dedalus.

The initial upper-layer flow is an along-channel Gaussian jet centered at x_c. The initial streamfunction is

$$\psi(t = 0) = -v_0\,L\;\mathrm{erf}\left(\frac{x - x_c}{L}\right)\,, \tag{10}$$

where erf is the error function,

$$\mathrm{erf}(\chi) \overset{\mathrm{def}}{=} \frac{2}{\sqrt{\pi}} \int_{\xi=0}^{\chi} e^{-\xi^2}\, d\xi\,, \tag{11}$$

$L/\sqrt{2}$ is the Gaussian decaying scale, v_0 is the jet maximum speed, and we recall that x_c is the x-coordinate of the lower-layer eddy center.

Based on Napolitano et al.'s (2019) shipboard observations of the BC in Tubarão Bight, we set $L = 25\,\mathrm{km}$, so that the jet width is 50 km. The AVISO analysis in section 2 reveals that the BC maximum speed in Tubarão Bight ranges from about 0.1 to about $0.5\,\mathrm{m\,s^{-1}}$ (figure 2). To study the model dependency on this variability, we conduct three sets of experiments with $v_0 = [0.1, 0.2, 0.5]\,\mathrm{m\,s^{-1}}$, representing a WEAK, MEAN, and STRONG BC regime. Figure 4 shows the model velocity profiles at $y = y_c$ for the lower-layer IWBC Eddy (dashed line) and the three selected velocities for the upper-layer BC jet (solid lines).

We choose a channel length long enough to prevent downstream-propagating anomalies from reentering the domain and spoiling the solutions in the lower-layer eddy region. Table 1 contains the parameters of all experiments discussed below. In these experiments, the channel width is 600 km, and the channel length varies from 2400 to 4800 km, with the longer channels for stronger jet experiments. The number

Table 1 Parameters used in the Dedalus experiments. For every experiment, we set an IWBC eddy radius r_e of 90 km and eddy speed v_e of $0.2\,\mathrm{m\,s^{-1}}$; we set the BC width to 50 km, and the jet position aligned with the IWBC eddy center. The deformation radius is 50 km.

Experiment		Channel		BC
name	ν	L^y	n^y	spd
	$(\mathrm{m^2\,s^{-1}})$	(km)		$(\mathrm{m\,s^{-1}})$
linear WEAK	02	2400	264	0.10
linear MEAN	04	2400	264	0.20
linear STRONG	12	2400	264	0.50
nonlinear WEAK	02	2400	264	0.10
nonlinear MEAN	04	3600	384	0.20
nonlinear STRONG	12	4800	512	0.50

of Chebyshev and Fourier modes are such that, in the middle of the domain, the grid space is $\Delta x \approx \Delta y \approx 10\,\mathrm{km}$. We tested the sensitivity of the solutions by running the model with double resolution and found only small differences.

We conduct both nonlinear and linear experiments for a WEAK, MEAN and STRONG upper-layer jet. The linear calculations are performed by suppressing the nonlinear term $J(\psi, \nabla^2\psi)$ from the full Jacobian $J(\psi, q)$ in (1), since $J(\psi, -Rd^{-2}\psi) = 0$.

4 Model results and discussion

Linear experiments

Figure 5 shows snapshots of streamfunction for the linear MEAN experiment ($v_0 = 0.2\,\mathrm{m\,s^{-1}}$). We only display the results for a region that extends about 300 km from the western boundary and about 450 km (150 km) south (north) of the lower-layer eddy. This channel strip is meant to represent the region between Abrolhos Bank (18 °S) and the Cape Frio High (24 °S), between the 200-m and 3500-m isobaths (see figure 1).

The dynamics here are governed by

$$q_t = -J\left(\psi, \frac{\psi_2}{R_d^2}\right) . \tag{12}$$

We emphasize that the tendency on the right of (12) is linear because ψ_2 is prescribed, and topographic steering by the lower-layer eddy drives changes in ψ. (The dissipation term $-\nu\nabla^2\zeta$ is negligible, and the solutions are essentially inviscid.) The evolution of the flow for the MEAN experiment in figure 5 is also typical for the other linear experiments (WEAK and STRONG, not shown), and differs from the parallel flow condition in (3), since the steady state approximation is relaxed and $q_t \neq 0$. The upper-layer jet immediately responds to the lower-layer eddy by developing a meander with a cyclone (a crest) upstream of the eddy center and an anticyclone (a trough) downstream of the eddy center. This wavy perturbation has a wavelength of about 40-50 km, is trapped and seems to propagate around the lower-layer eddy. With this trapped-wave propagation, the meander appears to wear down and form periodically. No steady state is achieved.

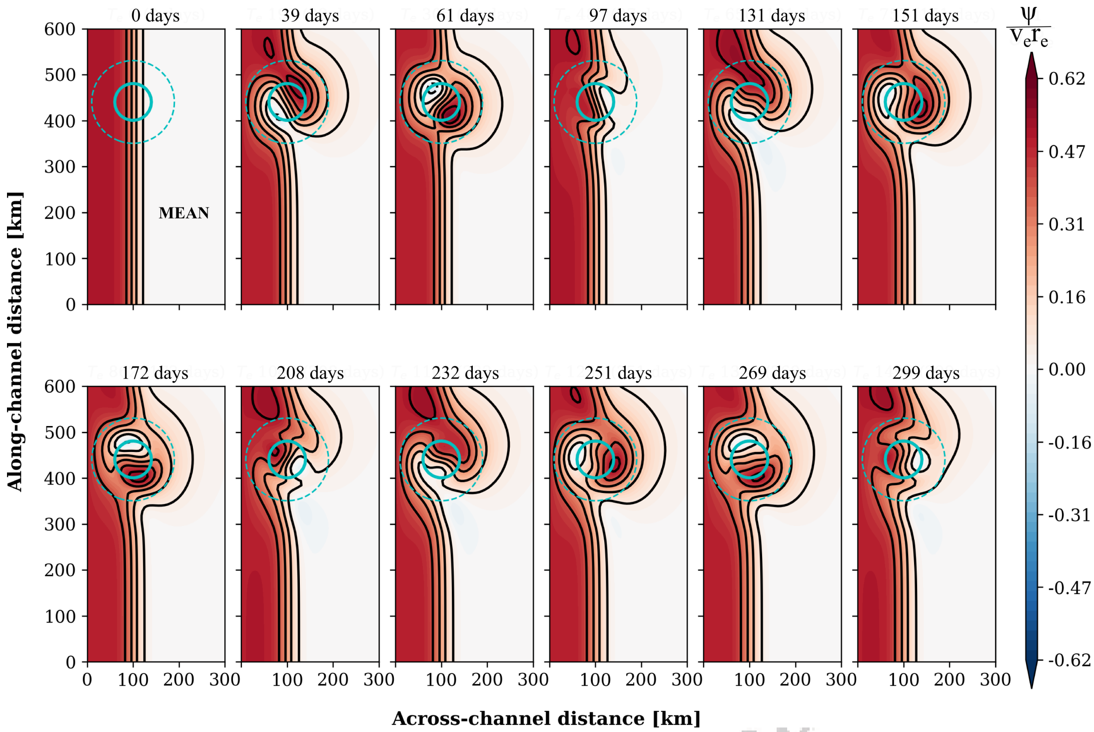

Fig. 5 Dedalus snapshots for ~300 days of simulation for the linear WEAK experiment. The colors and black streamlines represent the upper-layer modeled BC. The dashed cyan line represents the zero-velocity contour of the modeled lower-layer eddy, and the solid cyan contour represents the maximum eddy velocity.

In short, a stationary eddy (a Vitória Eddy) is not formed in the linear model, regardless the jet strength. We now turn to the evaluation of nonlinear solutions and discuss the parameters under which such eddy is formed.

Nonlinear experiments

Figure 6-A through 6-R show sequences of snapshots of the nonlinear evolution of the streamfunction for the cases of WEAK, MEAN, and STRONG upper-layer jet; all other flow parameters are fixed. In all three cases, the upper-layer jet quickly begins to meander in the lower-layer eddy region, but the solutions then begin to diverge. In the WEAK upper-layer jet case (figure 6-A to F), the meander grows to finite amplitude locally, with a strong cyclone (closed streamlines with $\psi > 0$) developing on top of the lower-layer eddy and an anticyclone (closed streamlines with $\psi < 0$) in the lee of the eddy (figure 6-C to F). The meander reaches its strongest amplitude in about 19 days (figure 6-D).

While the WEAK case leads to local meandering, the strong upper-layer jet rapidly advects the perturbation generated on top of the lower-layer eddy, which undergo explosive downstream growth (figure 6-G to L). In 17 days the cyclonic meander has grown to finite amplitude and travelled 300 km downstream (figure 6-

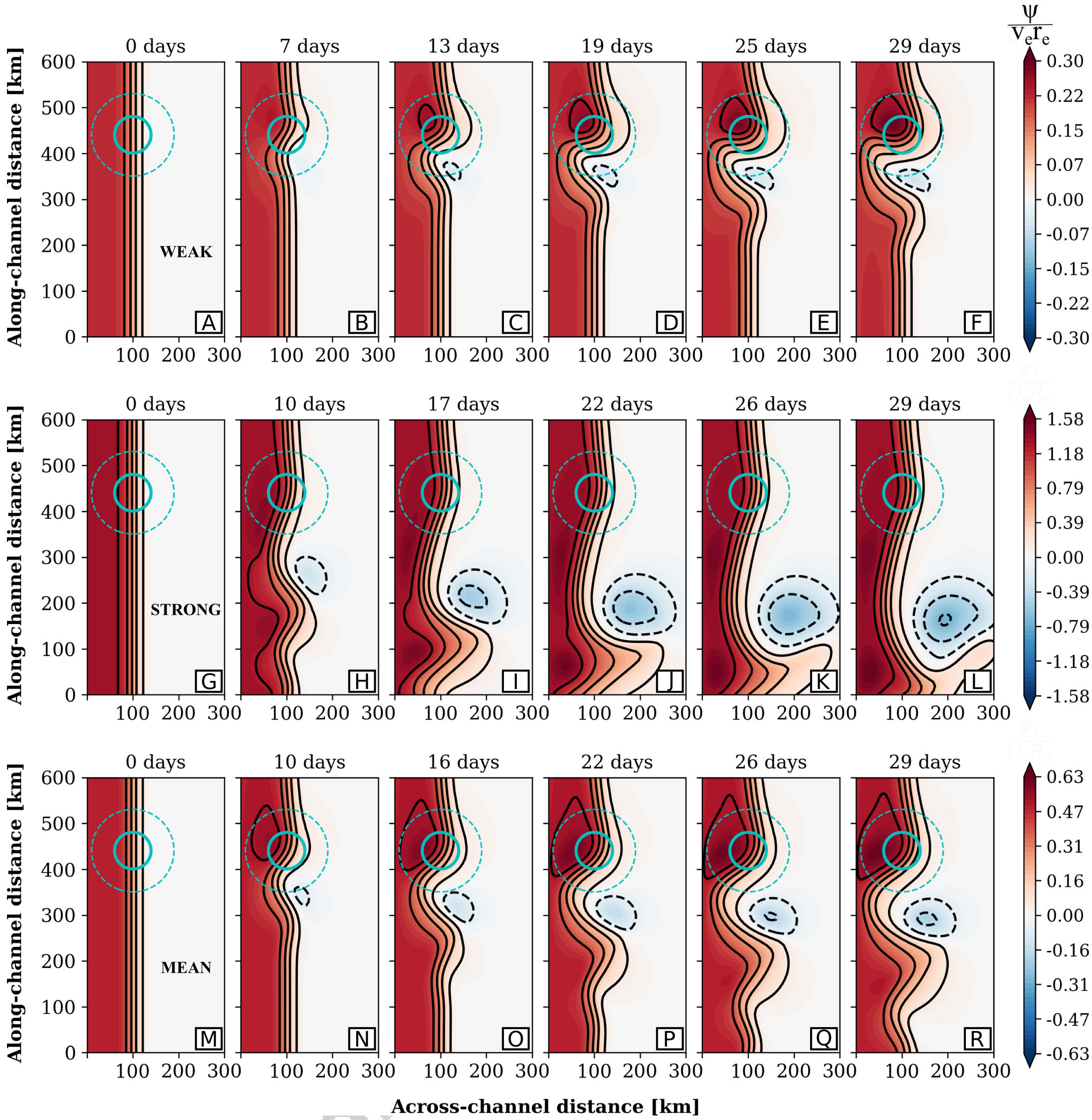

Fig. 6 Dedalus snapshots for ~30 days of simulation for the nonlinear (A-F) WEAK, (G-L) MEAN, and (M-R) STRONG experiments. The colors and black streamlines represent the upper-layer modeled BC. The dashed cyan line represents the zero-velocity contour of the modeled lower-layer eddy, and the solid cyan contour represents the maximum eddy velocity.

D). Interestingly, an anticyclonic vortex forms in the wake of the cyclonic meander. This vortex interacts nonlinearly with the meander, growing in amplitude as both features are advected downstream (see sequence in figures 6-I to L).

The MEAN upper-layer jet case displays features of these two extreme regimes (figure 6-M to R). The meander grows locally, but there is also downstream advection and growth. Given this partial downstream advection of the initial perturbations, the local meander has a smaller amplitude than in the WEAK case.

In cases where the eddy is formed, the anticyclonic part of the meander formed by the initial trigger (which is in the offshore part of the bump) is advected by the nonlinear term $J(\psi, \zeta)$. However, the cyclonic part of the meander remains trapped between the wall and the lower layer eddy stretching $J(\psi, \frac{\psi_2}{R_d^2})$.

Thus the jet velocity controls the magnitude of the nonlinear term $J(\psi, \zeta)$, which in turn drives changes in the flow: the stronger the upper-layer jet, the largest the initial $J(\psi, \zeta)$, and the faster the perturbations are advected downstream.

Our nonlinear quasi-steady solutions resemble the flow over topography problem discussed by Ingersoll (1969), who explored the formation of Taylor columns and the circulation around a topographic bump of different heights. Conversely, we vary the upper-layer jet velocity $v_0 = [0.1, 0.2, 0.5]\,\mathrm{m\,s^{-1}}$ and fix the "topographic bump" as an anomaly imposed by the steady lower-layer eddy (the IWBC Eddy),

$$h \stackrel{\text{def}}{=} \frac{h_b}{H} = \frac{\Psi_2}{f_0 R_d^2} = \frac{v_e}{f_0 R_d} \approx 0.08\,, \tag{13}$$

where $\Psi_2 = v_e R_d$ is the magnitude of the lower-layer streamfunction ($v_e = 0.2\,\mathrm{m\,s^{-1}}$ is the eddy velocity). With scales $R_d = 50\,\mathrm{km}$ and $f_0 = 5 \times 10^{-5}$, we obtain the Rossby number

$$R_o \stackrel{\text{def}}{=} \frac{v_0}{f_0 R_d} = [0.04, 0.08, 0.2] \tag{14}$$

for the WEAK, MEAN and STRONG upper-layer jet cases, respectively. Ingersoll (1969) remarks that a flat obstacle (a cylinder) yields solutions with closed streamlines when $h/R_o \geq 2$. In our experiments, we obtain closed streamlines not only with the weak upper-layer jet, where $h/R_o = 2$, but also in the MEAN case, where $h/R_o = 1$, possibly due to boundary effects.

A local steady state

We discussed above the first 30 days of simulations because it is the approximate time it takes for the meanders to reach finite amplitude locally or for the downstream meander to leave our region of interest. The changes after these 30 days are relatively small, and the solution slowly approaches an approximate steady state *within* the 300 × 600-km channel strip of the snapshot figures.

To assess the convergence of the solution to this local steady state, we define an iterative normalized root mean square streamfunction

$$RMS_\psi \stackrel{\text{def}}{=} \sqrt{\frac{\sum(\psi_i - \psi_{i-1})^2}{\sum \psi_i^2}}\,, \tag{15}$$

where i represents simulation days. A reasonable criterion to define a local steady state is that $RMS_\psi \leq 2 \times 10^{-3}$; i.e., the solution varies by less than 0.2% from the previous day.

Figure 7 shows timeseries of RMS_ψ for the BC nonlinear cases. The time taken to achieve an approximate steady state varies widely across the simulations. (Note the different time range in figures 7-A, B and C.) In the WEAK case, the solution reaches a steady state in 194 days (panel A), and in the MEAN case (panel

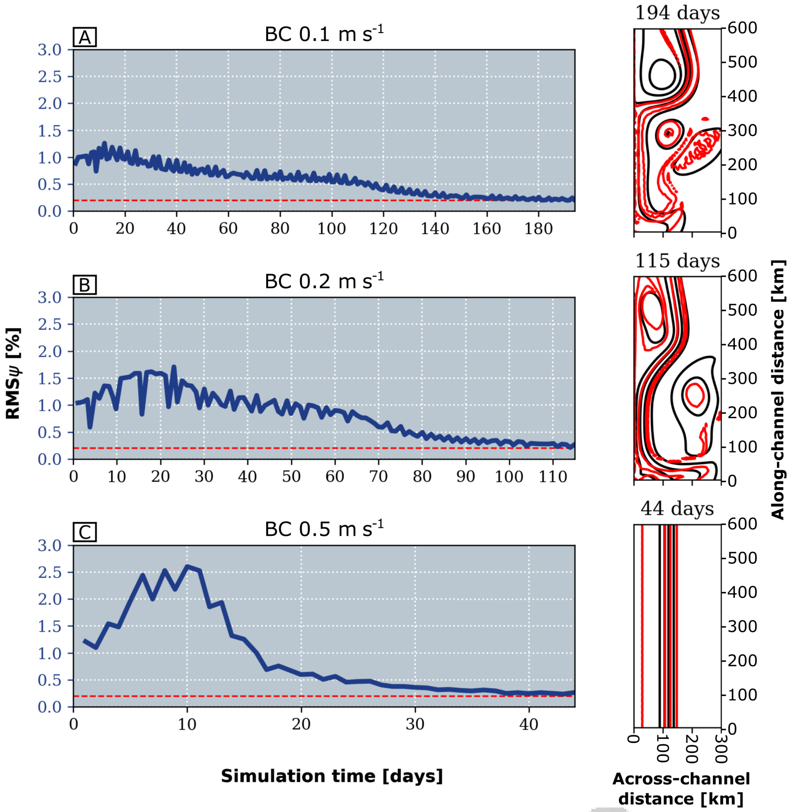

Fig. 7 Root mean square differences between daily streamfunction fields. In the left panels, the dashed red line represents the $2{\times}10^{-3}$ threshold; in the right panels, solid red lines represent potential vorticity and solid black lines represent streamfunction for (A) the WEAK BC, (B) the MEAN BC and (C) the STRONG BC.

B) it takes 115 days. In both cases the steady solution consists of a standing meander, with the jet deflecting toward the boundary downstream of the lower-layer eddy. On top of the lower-layer eddy, both solutions display closed contours of streamfunction and potential vorticity. Another common feature is a pinched-off anticyclonic eddy downstream of the meander and away from the boundary.

The strong upper-layer jet (STRONG BC, panel C) reaches an approximate steady state much faster, in about 44 days. While perturbations induced by the lower-layer eddy grow explosively as they are advected downstream, these transient eddies are swept out of the domain of interested. There are no closed contours of streamfunction and potential vorticity; the steady solution is a straight jet similar to the initial condition.

Linear vs nonlinear dynamics

We now step further into the dynamics of our nonlinear experiments to investigate the contribution of the linear relative to the nonlinear term of the solution for the

WEAK, MEAN, and STRONG cases. Expanding the Jacobian in the potential vorticity equation (1) yields

$$J(\psi, q) = \underbrace{J(\psi, \zeta)}_{\text{nonlinear}} + \underbrace{J(\psi, \psi_2/R_d^2)}_{\text{linear}}, \tag{16}$$

where we recall that $\zeta = \nabla^2\psi$ is the relative vorticity. The linear term on the right of (16) represents the steering of the upper-layer flow by the lower-layer eddy, and it scales as

$$\text{LINEAR} \sim R_d^{-4}\Psi\Psi_2 = R_d^{-2}v_0 v_e\,. \tag{17}$$

The nonlinear term is the advection of relative vorticity by the upper-layer flow, and it has magnitude

$$\text{NONLINEAR} \sim R_d^{-4}\Psi^2 = R_d^{-2}v_0^2\,. \tag{18}$$

In the above scaling we assumed that the eddy quantities have deformation radius length scales. The ratio between these two terms is

$$\frac{\text{LINEAR}}{\text{NONLINEAR}} \sim \frac{\Psi_2}{\Psi} = \frac{v_e}{v_0} = \frac{h}{R_o}\,, \tag{19}$$

where h is the non-dimensional amplitude of the lower-layer eddy, which is equivalent to a topographic Rossby number [see the discussion surrounding (13)].

For the WEAK case, this ratio is 2. Thus we expect that both terms are important, with the linear term dominating within the lower-layer eddy region. Figure 8-A displays an along-channel Hovmöller diagram of the potential vorticity tendency (q_t) through the center of the lower-layer eddy ($x = x_c$). The vertical dashed line is $y = y_c$, the center of the lower-layer eddy. Panels B and C of figure 8 breaks down this tendency into the contributions of the linear and nonlinear terms in (16). This linear term provides the initial trigger for the jet meandering in the lower-layer eddy region, with the upper-layer jet being steered by the lower-layer eddy. In the initial few days of the simulation, the linear term accounts for most of the potential vorticity tendency. Downstream of the lower-layer eddy, where the linear term vanishes, the nonlinear term takes over, with the formation of a strong anticyclonic eddy and the slow propagation of a small meander (see the slanted pink and green strips in figure 8-C). To quantify the relative importance of linear and nonlinear dynamics, we compute a timeseries of

$$\gamma \stackrel{\text{def}}{=} \frac{\text{rms(linear)}}{\text{rms(linear+nonlinear)}}\,, \tag{20}$$

where rms denotes root mean square. The ratio γ quantifies the relative importance of the linear and nonlinear terms, being 1 for fully linear and zero for fully nonlinear dynamics.

Figure 8-D shows this ratio for the WEAK experiment. As indicated in the Hovmöller diagrams, the dynamics are fully linear at the beginning of the meandering process, but nonlinear advection becomes important after one day, and it dominates the dynamics after 10 days.

Figures 8-E and F show the ratio γ for the MEAN and STRONG experiments. In all cases the initial trigger is a linear process—the steering of the upper-layer jet by the lower-layer eddy. But the nonlinear takeover occurs more rapidly with

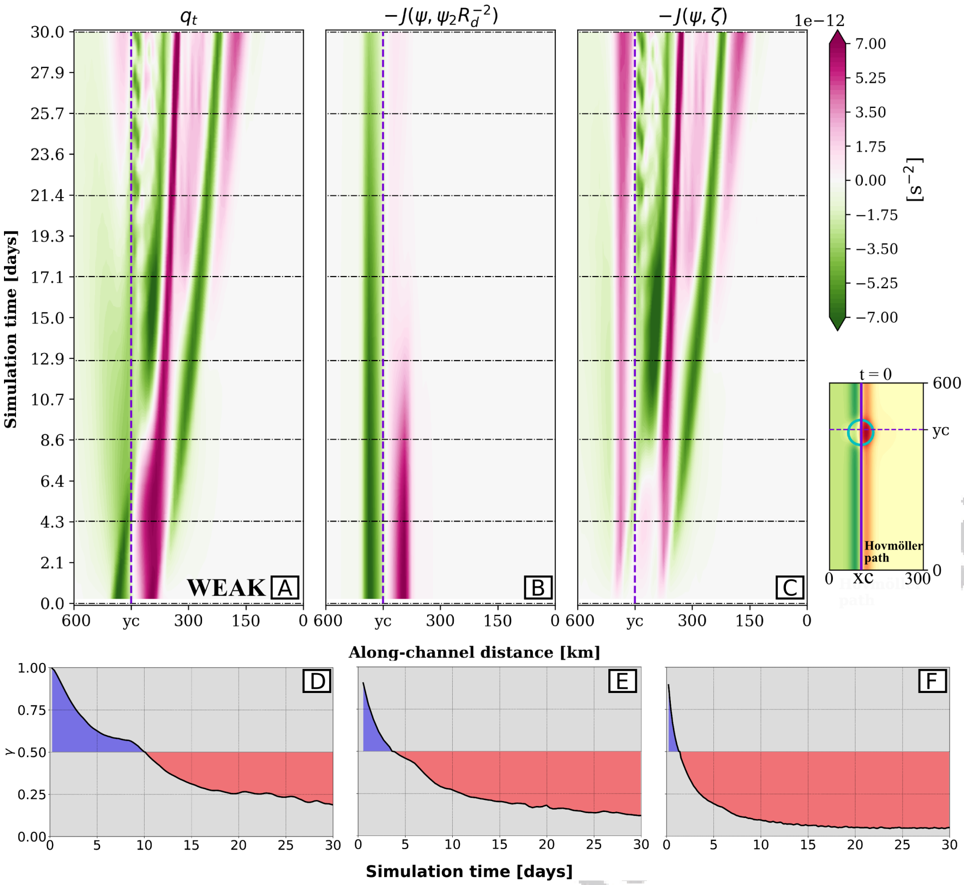

Fig. 8 Hovmöller diagram of (A) variation of potential vorticity, (B) linear term of the Jacobian, (C) nonlinear term of the Jacobian in (1) for the nonlinear WEAK BC experiment. The vertical dashed line represents the center of the eddy at yc, separating the dynamics upstream and downstream of the lower-layer eddy. Horizontal dashed lines represent timesteps of the analyzed snapshots. The potential vorticity at $t = 0$ is shown in the lower right. The time-series show the ratio between the linear and nonlinear terms throughout the simulation for (D) WEAK, (E) MEAN and (F) STRONG cases.

the increasing upper-layer jet speed (and associated reduction of the h/R_o parameter). For the STRONG upper-layer jet experiment, where the local meandering is weak and most of the variability is accounted for by downstream meander growth, nonlinear advection dominates after about 2 days, and after 15 days it accounts for essentially all the dynamics. In this STRONG case, after the initial trigger, the upper-layer jet barely feels the lower-layer eddy, and it satisfies standard two-dimensional dynamics $q_t \approx -J(\psi, \zeta)$.

5 Final remarks

Using a simple theoretical model, we show that the intermediate-layer IWBC recirculation may be strong enough to steer the Brazil Current, leading to the formation of the Vitória Eddy above this recirculation. Thus the topographically constrained intermediate flow likely influences the Brazil Current eddying circulation. Our model simulates the IWBC recirculation as a steady eddy that acts like a topographic bump in a barotropic model, and the Vitória Eddy formation is treated effectively as a flow past topography problem. Thus the Vitória Eddy can be addressed as a stagnant region in the solution, i.e., a Taylor-column.

Our model results suggest that the initial trigger for the Vitória Eddy is a linear process—the steering of the Brazil Current jet by the IWBC recirculation flow. But nonlinearity, through advection of the anticyclonic portion of relative vorticity anomaly generated by the linear topographic steering of the Brazil Current, is also needed for the Vitória Eddy growth. In the linear experiments, the Vitória Eddy does not form (figure 5). But in the nonlinear experiments, the steady IWBC recirculation steers the current. When the Brazil Current jet is relatively weak ($\leq 0.2\,\mathrm{m\,s^{-1}}$), a standing meander forms on top of the IWBC recirculation, and nonlinearity drives downstream meander growth (figures 6-A to F; and 6-M to R). In this case, downstream of the recirculation, the Brazil Current veers rapidly toward the boundary. In the local steady state the Brazil Current is attached to the boundary south of the Vitória Eddy (figure 7-A). When the Brazil Current is very strong ($0.5\,\mathrm{m\,s^{-1}}$; figure 6-G to L), the potential vorticity anomalies generated on top of the recirculation are quickly swept away, leading to explosive downstream meander growth. In this case, no Vitória Eddy is formed.

Given the complex structures and interactions depicted by our AVISO analysis (figure 3), our model cannot be used to fully explain the Vitória Eddy formation or to quantitatively represent the observed patterns. But it is certainly an initial step toward understanding the process. Future studies could add more complexity to the model, including changes in the upper-layer jet velocity, the Brazil Current feedback into the IWBC recirculation [i.e., adding an evolution equation for $v = v_0$ in (10) and for q_2, respectively]. Also, effects of topography, and eddy decay processes could be included. Recently, Napolitano et al. (2019) showed that the variability in the region is dominated by westward-propagating eddies, which are likely to complicate the picture. To further address the mechanisms that drive the Vitória Eddy, we call for a hierarchy of models, from solutions as simple as ours to idealized primitive-equation simulations to complex regional numerical models.

Acknowledgements We thank Frank O. Smith for copy editing and proofreading this manuscript. This study was financed in part by Coordenação de Aperfeiçoamento de Pessoal de Nível Superior—CAPES, Brazil—Finance Code 001 and by Projeto REMARSUL (Processo CAPES 88882.158621/2014-01), Projeto VT-Dyn (Processo FAPESP 2015/21729-4) and Projeto SUB-MESO (Processo CNPq 442926/2015-4). Altimeter products were produced by Ssalto/Duacs available at www.aviso.altimetry.fr/duacs/.

References

Andres M (2016) On the recent destabilization of the Gulf Stream path downstream of Cape Hatteras. Geophysical Research Letters 43(18):9836–9842, DOI 10.1002/2016GL069966

Arruda WZ, Campos EJD, Zharkov V, Soutelino RG, Silveira ICA (2013) Events of equatorward translation of the Vitoria Eddy. Continental Shelf Research 70:61–73, DOI https://doi.org/10.1016/j.csr.2013.05.004

Boebel O, Davis RE, Ollitrault M, Peterson RG, Richardson PL, Schmid C, Zenk W (1999) The intermediate depth circulation of the Western South Atlantic. Geophysical Research Letters 26(21):3329–3332

Burns KJ, Vasil GM, Oishi JS, Lecoanet D, Brown BP (2019) Dedalus: A Flexible Framework for Numerical Simulations with Spectral Methods. arXiv e-prints arXiv:1905.10388, 1905.10388

Campos EJD (2006) Equatorward translation of the Vitória Eddy in a numerical simulation. Geophysical Research Letters 33(22), DOI doi.org/10.1029/2006GL026997

Costa VS, Mill GN, Gabioux M, Grossmann-Matheson GS, Paiva AM (2017) The recirculation of the intermediate western boundary current at the Tubarão Bight–Brazil. Deep Sea Research Part I: Oceanographic Research Papers 120:48–60

Hurlburt HE, Hogan PJ (2008) The gulf stream pathway and the impacts of the eddy-driven abyssal circulation and the deep western boundary current. Dynamics of Atmospheres and Oceans 45(3-4):71–101

Hurlburt HE, Metzger EJ, Hogan PJ, Tilburg CE, Shriver JF (2008) Steering of upper ocean currents and fronts by the topographically constrained abyssal circulation. Dynamics of Atmospheres and Oceans 45(3-4):102–134

Ingersoll AP (1969) Inertial Taylor columns and Jupiter's great red spot. Journal of the Atmospheric Sciences 26(4):744–752

Mano MF, Paiva AM, Torres AR, Coutinho ALGA (2009) Energy Flux to a Cyclonic Eddy off Cabo Frio, Brazil. Journal of Physical Oceanography 39(11):2999–3010, DOI 10.1175/2009JPO4026.1

McWilliams JC (1977) A note on a consistent quasigeostrophic model in a multiply connected domain. Dynamics of Atmospheres and Oceans 1(5):427–441, DOI doi.org/10.1016/0377-0265(77)90002-1

Mill GN, da Costa VS, Lima ND, Gabioux M, Guerra LAA, Paiva AM (2015) Northward migration of cape são tomé rings, brazil. Continental Shelf Research 106:27–37

Müller TJ, Ikeda Y, Zangenberg N, Nonato LV (1998) Direct measurements of western boundary currents off Brazil between 20 S and 28 S. Journal of Geophysical Research: Oceans 103(C3):5429–5437

Napolitano DC, da Silveira ICA, Rocha CB, Flierl GR, Calil PHR, Martins RP (2019) On the steadiness and instability of the Intermediate Western Boundary Current between 24 and 18 S. Journal of Physical Oceanography 49(12):3127–3143, DOI 10.1175/JPO-D-19-0011.1

Phillips NA (1954) Energy transformations and meridional circulations associated with simple baroclinic waves in a two-level, quasi-geostrophic model. Tellus 6(3):274–286, DOI 10.1111/j.2153-3490.1954.tb01123.x

Qiu B, Chen S (2005) Variability of the Kuroshio Extension Jet, Recirculation Gyre, and Mesoscale Eddies on Decadal Time Scales. Journal of Physical Oceanography 35(11):2090–2103, DOI 10.1175/JPO2807.1

Rocha CB, Silveira ICA, Castro BM, Lima JAM (2014) Vertical structure, energetics, and dynamics of the Brazil Current System at 22 S–28 S. Journal of Geophysical Research: Oceans 119(1):52–69

Schmid C, Schäfer H, Zenk W, Podestá G (1995) The Vitória eddy and its relation to the Brazil Current. Journal of Physical Oceanography 25(11):2532–2546

Silveira IC, Calado L, Castro BM, Cirano M, Lima JAM, Mascarenhas AS (2004) On the baroclinic structure of the Brazil Current-Intermediate Western Boundary Current system at 22–23 S. Geophysical Research Letters 31(14):L14308, DOI 10.1029/2004GL020036

Silveira ICA, Lima JAM, Schmidt ACK, Ceccopieri W, Sartori A, Franscisco CPF, Fontes RFC (2008) Is the meander growth in the Brazil Current system off Southeast Brazil due to baroclinic instability? Dynamics of Atmospheres and Oceans 45(3-4):187–207, DOI 10.1016/j.dynatmoce.2008.01.002

Soutelino RG, Silveira IC, Gangopadhyay A, Miranda J (2011) Is the Brazil Current eddy-dominated to the north of 20 S? Geophysical Research Letters 38(3)

Vallis GK (2017) Atmospheric and Oceanic Fluid Dynamics: Fundamentals and Large-Scale Circulation, 2nd edn. Cambridge University Press, DOI 10.1017/9781107588417